



Article

Short-Range Correlated Magnetic Core-Shell CrO₂/Cr₂O₃ Nanorods: Experimental Observations and Theoretical Considerations

Ashish C. Gandhi ¹ , Tai-Yue Li ¹, Ting Shan Chan ² and Sheng Yun Wu ^{1,*}

¹ Department of Physics, National Dong Hwa University, Hualien 97401, Taiwan; acg.gandhi@gmail.com (A.C.G.); tim312508@gmail.com (T.-Y.L.)

² National Synchrotron Radiation Research Center, Hsinchu 97401, Taiwan; chan.ts@nsrrc.org.tw

* Correspondence: sywu@mail.ndhu.edu.tw; Tel.: +886-3-863-3717

Received: 14 March 2018; Accepted: 7 May 2018; Published: 9 May 2018



Abstract: With the evolution of synthesis and the critical characterization of core-shell nanostructures, short-range magnetic correlation is of prime interest in employing their properties to develop novel devices and widespread applications. In this regard, a novel approach of the magnetic core-shell saturated magnetization (CSSM) cylinder model solely based on the contribution of saturated magnetization in one-dimensional CrO₂/Cr₂O₃ core-shell nanorods (NRs) has been developed and applied for the determination of core-diameter and shell-thickness. The nanosized effect leads to a short-range magnetic correlation of ferromagnetic core-CrO₂ extracted from CSSM, which can be explained using finite size scaling method. The outcome of this study is important in terms of utilizing magnetic properties for the critical characterization of core-shell nanomagnetic materials.

Keywords: nanocrystalline materials; CrO₂/Cr₂O₃; core-shell nanorods; oxide materials

1. Introduction

A usual approach in nanoscience generally involves two steps: first, the fabrication and characterization of nanomaterials, and second, employing their properties for the development of novel devices and widespread applications. In recent years, the fabrication and critical characterization of core-shell nanostructures has attracted enormous attention because of their widespread applications [1–5]. The enormous progress made in the field of high-density recording and nanotechnology make the study of exchange bias (EB) ferromagnetic (FM)/Antiferromagnetic (AF) core/shell system important. Among different EB systems, exchange coupled CrO₂/Cr₂O₃ are the least explored nanostructures due to difficulty in the critical characterization of constitute phases [6–8]. CrO₂ is a half-metallic ferromagnetic (FM) [9] material with a Curie temperature (T_C) of ~394 K, well above room temperature, which was used widely as an information storage material for magnetic recording tapes [10,11]. Recently, the half-metallic properties [12] of CrO₂ such as spin-dependent magnet-transport [13,14], double exchange coupling interactions due to the self-doping effect [15], the large magnetoresistance effect [16,17], and anomalous transport properties [18], etc., have attracted enormous interest. On the other hand, Cr₂O₃ is a low-anisotropy easy axis antiferromagnetic (AF) material with a Neel temperature (T_N) of ~307 K [19,20]. It exhibits piezomagnetic and magnetoelectric effects, and can be used in a device involving EB coupling, which makes it a promising material for the future spintronic-based applications [21–23]. The core-shell CrO₂/Cr₂O₃ nanostructures can easily be formed even at room temperature simply by the surface reduction of CrO₂ to Cr₂O₃ when exposed to air for a prolonged period of time [24]. Such an insulating Cr₂O₃ surface layer was treated as a tunneling barrier between CrO₂ particles by EB coupling [25]. The interface-driven magnetoelectric

effect has also been reported from granular CrO₂ due to the formation of AF-Cr₂O₃ surface layer [26,27]. The core diameter d_{core} of CrO₂ and shell-thickness t_{shell} of Cr₂O₃ can be further tuned simply by a thermal treatment in an ambient atmosphere at an elevated temperature. With the increase of reduction temperature, the long-range AF spin correlation of the Cr₂O₃ phase strengthens at the expense of the core CrO₂ phase, resulting in a short-range FM spin correlation. Therefore, due to the reduction of CrO₂ to Cr₂O₃, the magnetic configuration of the system is expected to experience the coexistence and competition of AF and FM interactions. However, the most difficult part is its critical characterization, particularly estimating the values of d_{core} and t_{shell} parameters.

In this work, the effect of thermal treatment resulting in the surface reduction of CrO₂ nanorods (NRs) to Cr₂O₃ phase is studied via the Rietveld refined X-ray diffraction (XRD) spectra and magnetic measurements. We have demonstrated utilization of magnetic properties of FM-CrO₂ as a tool to estimate the values of d_{core} and t_{shell} of CrO₂/Cr₂O₃ core-shell NRs. The observed finite size scaling behavior from core diameter d_{core} the dependency of T_C , confirmed the validity of used magnetic property-based theoretical expression.

2. Synthesis of CrO₂/Cr₂O₃ Nanostructures

In the synthesis of CrO₂-core with Cr₂O₃-shell NRs, we have carried out the reduction of pristine CrO₂ NRs simply by thermal treatment at 450, 500, 550, and 600 °C for a duration of 1 h in an ambient atmosphere. The pristine CrO₂ NRs were obtained commercially from Sigma-Aldrich (St. Louis, MO, USA) under the name of Magnetrieve. The reduction is carried out in a tube furnace with a heating rate of 5 K/min and allowed to cool down naturally. Note that thermal treatment at and above 650 °C resulted in a complete reduction of CrO₂ into pure AF Cr₂O₃ phase [28]. Structural properties were studied using synchrotron radiation XRD (SRXRD) ($\lambda = 0.7749 \text{ \AA}$) at National Synchrotron Radiation Research Center (NSRRC) beamline BL01C2 in Taiwan. Further analysis of the structural properties was carried out by selective area diffraction pattern (SAED) using JEOL 2010 TEM (Peabody, MA, USA) working at 200 kV. The analysis of SAED pattern was done by CaRIne Crystallography 3.1 software. Field-emission scanning electron microscopy (FE-SEM, JEOL JSM-6500F, Peabody, MA, USA) was utilized for the estimation of diameter distribution and morphological analysis. The mean diameter distribution was estimated from relative SEM images using Nano Measurer version 1.2.5. The temperature dependences of zero-field-cooled (ZFC) and field-cooled (FC) magnetization, thermoremanent magnetization (TRM) decay, and isothermal field dependences of magnetization measurements were carried out using a quantum design MPMS-SQUID-VSM magnetometer (San Diego, CA, USA).

3. Results and Discussion

3.1. X-ray Diffraction Analysis

Figure 1 displays the SRXRD spectra for the pristine CrO₂ NRs and 450, 500, 550, and 600 °C samples (spectra are shifted vertically for clear visibility). The diffraction spectrum of the pristine NRs is assigned to pure CrO₂ phase indexed with space group P4₂/mnm [25]. Along with CrO₂ phase, SRXRD spectra of 450 °C sample display additional peaks assigned to Cr₂O₃ phase indexed with space group R3-c [28]. 500, 550, and 600 °C samples do not show any noticeable diffraction peaks for CrO₂ phase, as can be clearly visualized from magnified spectrum shown in the supporting Figure S1a. For further detailed structural analysis, Rietveld [29] refinement of SRXRD spectra was carried out using GSAS [30] software package. The solid black line in Figure 1 is the fitted curve, and fitting parameters are tabulated in Supporting Table S1. From Rietveld refinement, we confirm that (i) only CrO₂ phase ($a = b = 4.4215 \text{ \AA}$, $c = 2.9177 \text{ \AA}$) existed in the pristine sample; (ii) both CrO₂ ($a = b = 4.4715 \text{ \AA}$, $c = 2.9206 \text{ \AA}$; weight fraction 0.33%) and Cr₂O₃ ($a = b = 4.9595 \text{ \AA}$, $c = 13.5684 \text{ \AA}$; weight fraction 99.67%) phases existed in 450 °C sample; and (iii) only Cr₂O₃ phase existed in 500 to 600 °C samples. The variation in the lattice constant ($a = b, c$) of Cr₂O₃ phase with respect to the annealing

temperature (T_A) is depicted in supporting Figure S1b. As compared to bulk Cr_2O_3 ($a = b = 4.959 \text{ \AA}$, $c = 13.589 \text{ \AA}$), sample reduced at $450 \text{ }^\circ\text{C}$ shows a noticeable lattice contraction along c -axis, whereas lattice constants along a -, b -axis have a value close to bulk. The observed contraction along c -axis could be attributed to finite size effect or defects [28].

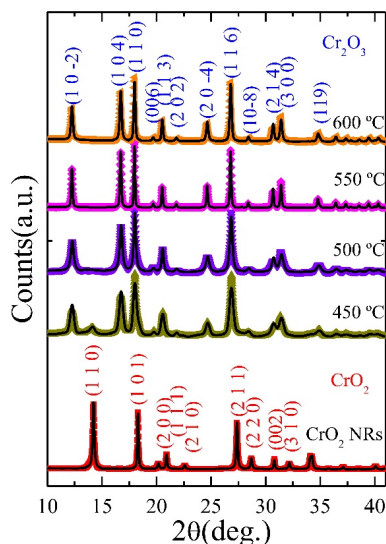


Figure 1. Synchrotron radiation XRD spectra of pristine CrO_2 and $450 \text{ }^\circ\text{C}$ to $600 \text{ }^\circ\text{C}$ NRs (bottom to top), in which solid curve represents the Rietveld fit to the SRXRD spectrum.

3.2. Morphological and Structural Analysis

The SEM images in Figure 2a–e show the nanorod-like morphology of pristine and 450 , 500 , 550 , and $600 \text{ }^\circ\text{C}$ samples, respectively. The effect of reduction resulted in the increase of NRs diameter, but with relatively smaller length than that of pristine NRs. The mean diameter $\langle d \rangle$ of the asymmetrically distributed NRs can be obtained by fitting log-normal distribution function:

$$f(d) = \frac{1}{\sqrt{2\pi}d\sigma} \exp \left[-\frac{(\ln d - \ln \langle d \rangle)^2}{2\sigma^2} \right]$$

in which σ is a standard deviation of the fitted function to the histogram of NRs diameter obtained from SEM images (Figure 2f–j). The fitted values of ($\langle d \rangle$, σ) of CrO_2 NRs and 450 , 500 , 550 , and $600 \text{ }^\circ\text{C}$ samples are ($24 \pm 1 \text{ nm}$, $0.16 \pm 0.02 \text{ nm}$), ($28 \pm 1 \text{ nm}$, $0.23 \pm 0.03 \text{ nm}$), ($31 \pm 1 \text{ nm}$, $0.28 \pm 0.08 \text{ nm}$), ($33 \pm 2 \text{ nm}$, $0.29 \pm 0.05 \text{ nm}$), and ($35 \pm 2 \text{ nm}$, $0.26 \pm 0.01 \text{ nm}$), respectively. As an effect of the increase of T_A , the mean diameter of $\text{CrO}_2/\text{Cr}_2\text{O}_3$ NRs increases and the diameter distribution widens. These changes could also be accompanied by an increase of reduction rate of CrO_2 to Cr_2O_3 with the increase of T_A [31]. Note that thermal reduction at $650 \text{ }^\circ\text{C}$ resulted in the formation of pure Cr_2O_3 NRs with $\langle d \rangle = 35 \pm 1 \text{ nm}$ [28].

For further structural characterization, the SAED pattern of pristine NRs, reduced samples, and Cr_2O_3 NRs [28] was examined. The SAED patterns in Figure 2k can be ascribed to the tetragonal- CrO_2 oriented along the $[100]$ zone axis. Interestingly, along with $450 \text{ }^\circ\text{C}$, the SAED pattern of 500 , 550 , and $600 \text{ }^\circ\text{C}$ samples displayed the existence of mix crystalline phases, as shown in Figure 2l–o. The observed mix phases in CrO_2 -reduced samples were ascribed to the tetragonal- CrO_2 and hexagonal- Cr_2O_3 phases oriented along the $[100]$ and $[-101]$ zone axis, respectively. However, observed mixed phase SAED pattern of 500 , 550 , and $600 \text{ }^\circ\text{C}$ samples contradict with the SRXRD spectra in which only Cr_2O_3 phase was noted, since SAED is a local technique and hence gives structural information only from a limited area. On the contrary, SRXRD, which is a global technique, gives average structural information. In 500 to $600 \text{ }^\circ\text{C}$ reduced samples, the weight percent of CrO_2 is

<0.33%, which is far below the SRXRD detection limit of ~1%. Similar discrepancy was also reported in our previous work on 14 nm Ni/NiO nanoparticles in which tiny amount of Ni phase (<0.7%) was detected through SAED and static/dynamic magnetic measurements but was hard to be detected using SRXRD [32]. Since magnetic moment of FM-CrO₂ is about 10,000 times that of AF-Cr₂O₃, in order to gain a detailed understanding of thermal reduction effects on CrO₂ NRs, we have carried out both field- and temperature-dependent magnetization measurements.

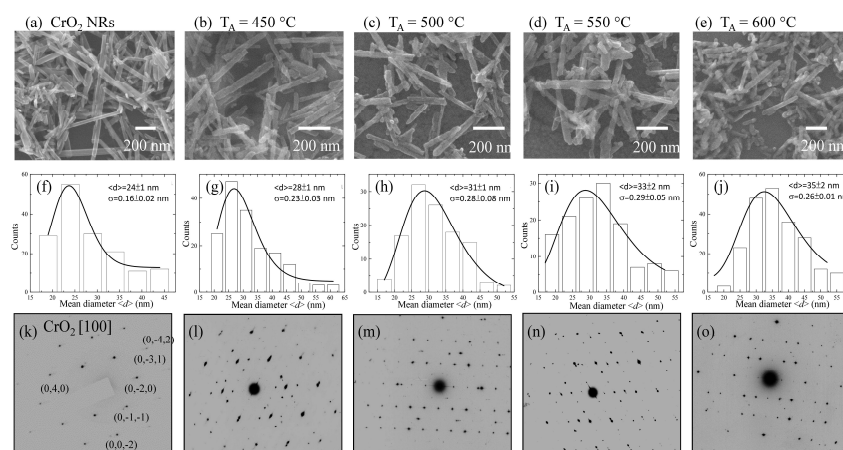


Figure 2. (a–e) SEM images; (f–j) histogram of diameter distribution and (k–o) SAED patterns of the CrO₂/Cr₂O₃ core-shell NRs. The line in (f–j) represents fit to the histogram using log-normal distribution function.

3.3. Determination of Core-Diameter and Shell-Thickness from the Saturated Magnetization

In the core-shell magnetic nanomaterials, usually, a large variety of possible magnetic behaviors can be encountered that vary with the type of material, the magnetic system (FM, ferrimagnetic, AF, superparamagnetic, etc.), inter- and intra-particle interactions, interface coupling, size, and morphologies. In such complex systems, it is very difficult to distinguish the intrinsic physical properties with respect to the size that is often obtained only from few nanowires or nanoparticles using TEM or SEM images. Therefore, from the macroscopic point of view, necessity of a characteristic magnetic ‘fingerprint’ arises such that different magnetic core-shell systems can be classified and distinguished to determine the core-diameter and shell-thickness. Saturated magnetization is a good candidate for a fingerprint for the FM-AF core-shell nanosized system. In general, according to Néel, the thermal fluctuations will affect the magnetization of a single domain ferromagnetic particle, resulting in its decay towards the thermal equilibrium. However, he has neglected the contribution from magnetic anisotropy. Later, Néel-Brown introduces a thermally activated magnetization reversal model to describe a single domain magnetic particle with two equivalent ground states of opposite magnetization separated by an energy barrier, which is due to the shape and crystalline anisotropy. Within the framework, we establish a core-shell saturated magnetization (CSSM) cylinder model to describe the moment contribution in saturated magnetization at the lowest temperature. A schematic of the side view and cross view of thermally reduced core-shell nanorod is shown in Figure 3a, such that atoms of Cr₂O₃-shell and CrO₂-core give rise to a net surface macro-moment m_2 and a net inner macro-moment m_1 . Quantitative analysis for the CSSM was applied to the saturated magnetization M_S at various annealing temperatures T_A , as shown in Figure 3b. In the theoretical modeling, we assume that contribution from the magnetic moments of Cr₂O₃ phase to the saturation magnetization (M_S) in CrO₂/Cr₂O₃ core-shell NRs is very weak, such that it can be neglected, and therefore only FM-CrO₂ phase contributes to the M_S . We propose that the saturated magnetization at the lowest temperature, which was computed from the saturated moment divided by the mass of CrO₂ content from elemental analysis, can be described as

$$\frac{M_S}{M_S^{CrO_2}} = \left[\frac{N_{CrO_2}}{N_{CrO_2} + N_{Cr_2O_3}} \right] \tag{1}$$

in which $M_S^{CrO_2}$ is the saturation magnetization of CrO_2 NRs. N_{CrO_2} and $N_{Cr_2O_3}$ are the average number of CrO_2 and Cr_2O_3 atoms per gm at the core and in the shell, which can be calculated using bulk densities (δ) of CrO_2 and Cr_2O_3 (4.89 g/cm³, 5.22 g/cm³) as

$$N_{CrO_2} = \delta_{CrO_2} V_{CrO_2} N_A \tag{2}$$

$$N_{Cr_2O_3} = \delta_{Cr_2O_3} V_{Cr_2O_3} N_A = c \delta_{CrO_2} V_{Cr_2O_3} N_A \tag{3}$$

in which $c = \frac{\delta_{Cr_2O_3}}{\delta_{CrO_2}}$; N_A is Avogadro's number. Combining Equations (1)–(3) gives

$$\frac{V_{CrO_2}}{V_{CrO_2} + cV_{Cr_2O_3}} = \frac{M_S}{M_S^{CrO_2}} \tag{4}$$

considering that a CrO_2/Cr_2O_3 core-shell NRs has a concentric cylinder, the total radius (r) will be given by the sum of core radius (r_1) and shell thickness (t), as shown in Figure 3a. The volume of a cylinder is given by $V = \pi r^2 l$, in which l is a length of the nanorod. Considering n as any positive number, the length of a cylinder can be expressed as $l = nr$. The volume of core and shell can be written separately as $V_{CrO_2} = \pi r_1^2(nr - 2t)$ and $V_{Cr_2O_3} = \pi nr^3 - V_{CrO_2} = \pi nr^3 - \pi r_1^2(nr - 2t)$, respectively, and, combined with Equation (4), we can obtain a relation between the thickness and saturated magnetization as

$$t = r \left[1 - \frac{1}{\sqrt{\frac{(nr-2t)}{nr} \left[\left(\frac{M_S^{CrO_2}}{cM_S} - \frac{1}{c} \right) + 1 \right]}} \right] \tag{5}$$

The nanorod length is much larger than the shell thickness; we can take $(nr - 2t) \approx nr$, which resulted in the simplified CSSM model as

$$t = r \left[1 - \frac{1}{\sqrt{\left(\frac{M_S^{CrO_2}}{cM_S} - \frac{1}{c} \right) + 1}} \right] \tag{6}$$

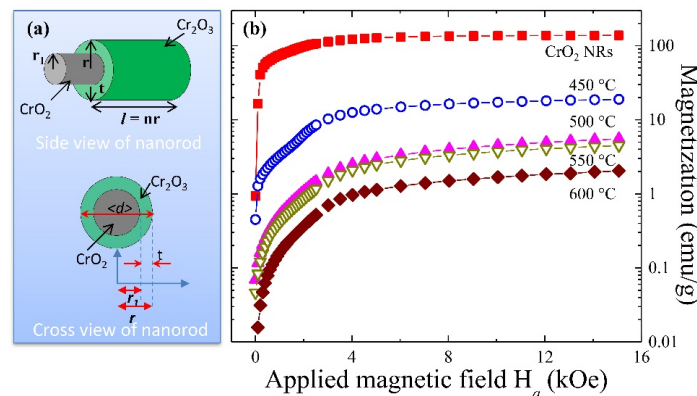


Figure 3. (a) A schematic illustration of side- and cross-view of CrO_2/Cr_2O_3 core-shell nanorod; (b) magnetization versus applied magnetic field of CrO_2 and 450 to 600 °C NRs measured at 2 K from 0 to 15 kOe.

Above expression gives the useful relation between the Cr_2O_3 shell thickness t and the total radius $r = d_{\text{core}}/2 + t$ of $\text{CrO}_2/\text{Cr}_2\text{O}_3$ core-shell NRs. The above simplified CSSM model was used to calculate Cr_2O_3 shell thickness and CrO_2 core diameter as tabulated in Supporting Table S2. As shown in Figure 4, the core diameter d_{core} decreases with the increase of annealing temperature T_A , which can be described very well by fitting an exponential decay function $d_{\text{core}} = d_{\text{co}} + \rho \exp(-T_A/T_{\text{CO}})$, in which $d_{\text{co}} = 1.13 \pm 0.03$ nm, $\rho = 200$ nm, and $T_{\text{CO}} = 145 \pm 12$ °C represent the initial constants and the fitted parameters, respectively. The observed linear increasing behavior of Cr_2O_3 shell thickness can be described using growth function $t = t_0 + \gamma T_A$, in which $t_0 = -9.6 \pm 3.8$ nm and $\gamma = 0.042 \pm 0.007$ nm/°C. The above finding indicates that the surface reduction of CrO_2 to Cr_2O_3 begins around $T_A \sim 229$ °C, and a self-terminated layer of ~ 17.5 nm was obtained at $T_A \sim 650$ °C [28]. It is noteworthy that the shell thickness can also be estimated from TEM results, but with less accuracy, because CrO_2 NRs on TEM substrate film are more susceptible to oxidation than samples for magnetometer measurement that were stored in a capsule.

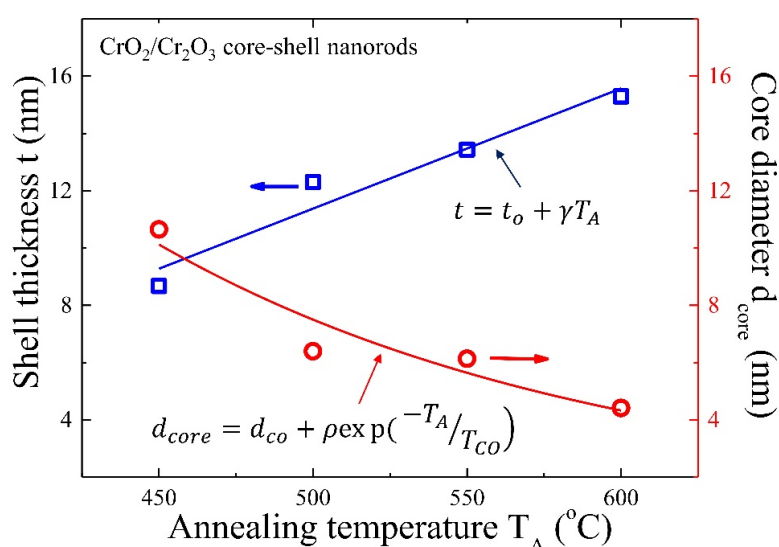


Figure 4. A plot of the T_A dependence of the obtained shell thickness t and the core diameter d_{core} . The solid curves represent linear and exponential fits to the experimental data.

3.4. Temperature Dependence of Thermoremanent Magnetization (TRM)

In general, in a superparamagnetic (SPM) nanoscaled system, thermoremanence is related to the distribution of energy barriers. At a given measuring temperature and after removing the applied field, only the particles that are in the blocked regime will contribute to the remanent magnetization. To estimate the effect of thermal treatment on T_C of CrO_2 phase, TRM decay measurements of 450 to 600 °C samples were undertaken. Initially, sample was cooled down from 350 to 1.8 K under an applied magnetic field of $H_a = 100$ Oe. Once temperature stabilized, the magnetic field was switched off using oscillating mode, and subsequently magnetization decay with respect to temperature T was recorded while warming the sample in a zero field. Figure 5 shows the normalized plot of TRM curve, indicating the presence of irreversible contributions in the low-temperature region. A monotonically decreasing behavior reflecting the expected thermally induced decay of magnetization was observed and vanished above a characteristic temperature. The value of T_C from $\text{CrO}_2/\text{Cr}_2\text{O}_3$ core-shell NRs was obtained by fitting TRM curve using $M(T) = M_0(1 - T/T_C)^\alpha$, in which α is a power law factor. The solid line in Figure 5 represents the fitted curve using above expression, and fitting parameters are tabulated in Supporting Table S2. The fitted value of T_C matches with ferromagnetic ordering temperature, which marks the ordering temperature of the FM cores, i.e., 321 ± 5 , 281 ± 5 , 271 ± 15 , and 191 ± 14 K for $\langle d \rangle = 28, 31, 33,$ and 35 nm NRs, respectively. The amount of reduction of CrO_2 to

Cr_2O_3 increases with the increase of T_A up to 600°C , above which a pure Cr_2O_3 phase was obtained. Therefore, observed decreases of T_C with an increase of T_A could be resulted from the finite size effect, which will be discussed further in the text. The value of $T_C \sim 388\text{ K}$ of pristine CrO_2 NRs is defined from a point at which ZFC-FC curve overlaps and above which it retains superparamagnetic behavior such as magnetization decay with the increase of T as shown in the inset of Figure 5. Note that obtained value of T_C from pristine CrO_2 NRs is very close to the report value of 394 K .

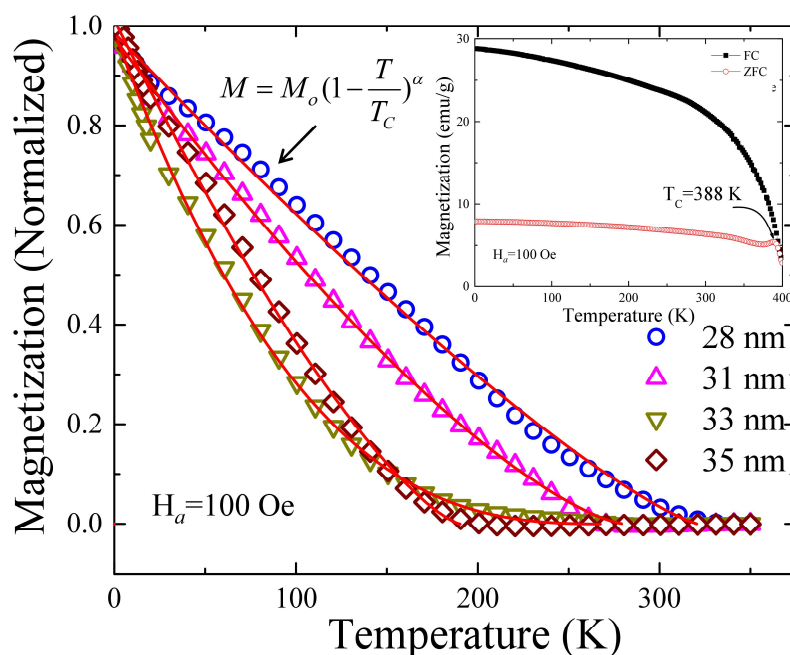


Figure 5. Temperature dependency of thermoremanent magnetization of 450 to 600°C NRs. The solid curve represents a fit using a model given in the text. Inset of the figure shows the ZFC-FC curve of pristine CrO_2 NRs.

3.5. Finite Size Scaling Method

The values of T_C decrease from 388 to 191 K with the decrease of CrO_2 diameter d_{core} from 24 to 4.42 nm as shown in Figure 6, signaling a strong size effect. In a nanoscaled FM-core system, the finite size scaling method can be used to extract the values for the critical exponents by observing how measured quantities vary as the size d of the system studied changes. However, the technique we used for those calculations required us to perform simulations exactly at the critical temperature of the model, which in turn requires us to know T_C . The diameter dependence of T_C can be explained using finite size scaling formula [33] $T_C(d) = T_C(\infty) \left[1 - \left(\frac{\zeta_0}{d_{core}} \right)^\beta \right]$, in which $T_C(\infty) = 394\text{ K}$ for bulk CrO_2 , ζ_0 is the characteristic microscope dimension of the system at zero temperature, and the exponent is related to the correlation length by $\beta = 1/\lambda$. Fitting T_C vs. d_{core} of core-shell NRs yields $\zeta_0 = 3.1 \pm 0.2\text{ nm}$, which is roughly ~ 0.70 and ~ 1.06 times the lattice constant $a = b$ and c . The value of the characteristic microscopic length scale indicates that growth of CrO_2 NRs is along the c -axis. The obtained value $\lambda = 0.56$ ($\beta = 1.8 \pm 0.2$) is close to the value predicted using isotropic 3D Heisenberg model ($0.65 \leq \lambda \leq 0.733$) [34]. Above finding shows that the finite size scaling formula can efficiently describe the shift in T_C , giving validation of used magnetic property-based theoretical expression for the estimation of core and shell parameters.

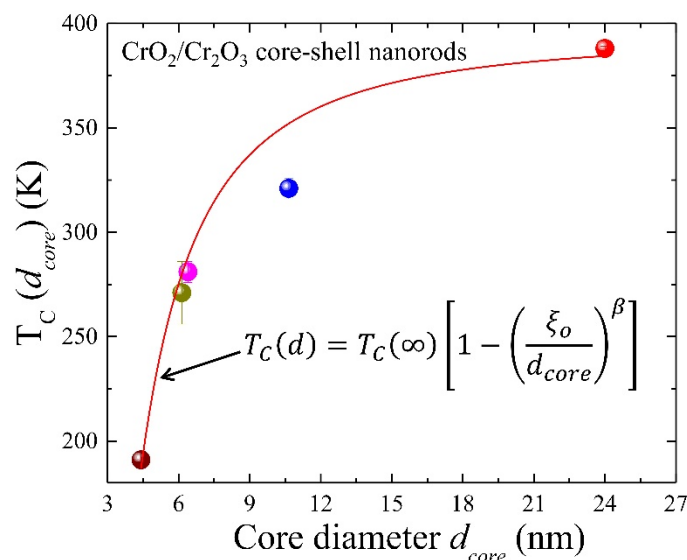


Figure 6. A plot of core diameter d_{core} dependence of the T_C , in which solid curve represents a fit using finite size scaling model discussed in the text.

4. Conclusions

The series of $\text{CrO}_2/\text{Cr}_2\text{O}_3$ core-shell NRs with mean diameters varying from 28 to 35 nm were synthesized simply by thermal reduction technique. A new approach by means of DC magnetometer and a core-shell saturated magnetization (CSSM) cylinder model has been proposed for the estimation of core- CrO_2 diameter and shell- Cr_2O_3 thickness, which is otherwise impossible to calculate using any conventional means. We observed that with the increase of reduction temperature from 450 to 600 °C, core- CrO_2 diameter reduced from ~11 to 4 nm and shell- Cr_2O_3 thickness increased from ~9 to 15 nm, respectively. Finite size effect of FM- CrO_2 leads to reduced Curie temperature T_C of NRs, which can be explained further using the finite size scaling model, giving a short-range magnetic correlation length of $= \xi_0$ 3.1 ± 0.2 nm. This work is believed to be of importance, especially for researchers working on the magnetic core-shell nanostructures and their application in functional devices.

Supplementary Materials: The following are available online at <http://www.mdpi.com/2079-4991/8/5/312/s1>.

Author Contributions: S.Y.W. and A.C.G. wrote, conceived, and designed the experiments. A.C.G., T.-Y.L., and T.S.C. analyzed the data. T.S.C. contributed the experimental facilities for the X-ray measurements. All authors discussed the results, contributed to the text in the manuscript, commented on the manuscript, and approved the final version.

Acknowledgments: We would like to thank the Ministry of Science and Technology (MOST) of the Republic of China for their financial support of this research through project numbers MOST-106-2112-M-259-001 and 106-2731-M-259-001.

Conflicts of Interest: The authors declare no conflict of interest.

References

1. Velasquez, E.A.; Lopez-Moreno, S.; Mazo-Zuluaga, J.; Mejia-Lopez, J. Fe/Ni core-shell nanowires and nanorods: A combined first-principles and atomistic simulation study. *Phys. Chem. Chem. Phys.* **2017**, *19*, 16267–16275. [[CrossRef](#)] [[PubMed](#)]
2. Gandhi, K.; Chaudhary, R.P.; Mohapatra, J.; Koymen, A.R.; Liu, J.P. Giant exchange bias and its angular dependence in Co/CoO core-shell nanowire assemblies. *Phys. Lett. A* **2017**, *381*, 2092–2096. [[CrossRef](#)]
3. Salazar-Alvarez, G.; Geshev, J.; Agramunt-Puig, S.; Navau, C.; Sanchez, A.; Sort, J.; Nogués, J. Tunable High-Field Magnetization in Strongly Exchange-Coupled Freestanding Co/CoO Core-Shell Coaxial Nanowires. *ACS Appl. Mater. Interface* **2016**, *8*, 22477–22483. [[CrossRef](#)] [[PubMed](#)]

4. Liébana-Viñas, S.; Wiedwald, U.; Elsukova, A.; Perl, J.; Zingsem, B.; Semisalova, A.S.; Salgueiriño, V.; Spasova, M.; Farle, M. Structure-Correlated Exchange Anisotropy in Oxidized Co₈₀Ni₂₀ Nanorods. *Chem. Mater.* **2015**, *27*, 4015–4022. [[CrossRef](#)]
5. Javed, K.; Li, W.J.; Ali, S.S.; Shi, D.W.; Khan, U.; Riaz, S.; Han, X.F. Enhanced exchange bias and improved ferromagnetic properties in Permalloy-BiFe_{0.95}Co_{0.05}O₃ core-shell nanostructures. *Sci. Rep.* **2015**, *5*, 18203. [[CrossRef](#)] [[PubMed](#)]
6. Singh, G.P.; Ram, S. Optical and electron paramagnetic resonance properties of native Cr₂O₃ surface over CrO₂. *J. Magn. Magn. Mater.* **2010**, *322*, 1484–1487. [[CrossRef](#)]
7. Zhao, Q.; Wen, G.; Liu, Z.; Yuan, J.; Li, D.; Zou, G.; Zheng, R.; Ringer, S.P.; Mao, H.-K. High-density, vertically aligned crystalline CrO₂ nanorod arrays derived from chemical vapor deposition assisted by AAO templates. *Chem. Commun.* **2009**, *14*, 3949–3951. [[CrossRef](#)] [[PubMed](#)]
8. Dho, J.; Ki, S.; Gubkin, A.F.; Park, J.M.S.; Sherstobitova, E.A. A neutron diffraction study of half-metallic ferromagnet nanorods. *Solid State Commun.* **2010**, *150*, 86–90. [[CrossRef](#)]
9. Schwarz, K. CrO₂ predicted as a half-metallic ferromagnet. *J. Phys. F Met. Phys.* **1986**, *16*, L211. [[CrossRef](#)]
10. Coey, R.; Skomski, J.M.D. *Permanent Magnetism*; Taylor & Francis: New York, NY, USA, 1999.
11. Skomski, R. *Simple Models of Magnetism*; Oxford University Press: Oxford, UK, 2008.
12. Solovyev, I.V.; Kashin, I.V.; Mazurenko, V.V. Mechanisms and origins of half-metallic ferromagnetism in CrO₂. *Phys. Rev. B* **2015**, *92*, 144407. [[CrossRef](#)]
13. Coey, J.M.D.; Berkowitz, A.E.; Balcells, L.; Putris, F.F.; Barry, A. Magnetoresistance of Chromium Dioxide Powder Compacts. *Phys. Rev. Lett.* **1998**, *80*, 3815–3818. [[CrossRef](#)]
14. Dai, J.; Tang, J. Junction-like magnetoresistance of intergranular tunneling in field-aligned chromium dioxide powders. *Phys. Rev. B* **2001**, *63*, 054434. [[CrossRef](#)]
15. Shim, J.H.; Lee, S.; Dho, J.; Kim, D.-H. Coexistence of Two Different Cr Ions by Self-Doping in Half-Metallic CrO₂ Nanorods. *Phys. Rev. Lett.* **2007**, *99*, 057209. [[CrossRef](#)] [[PubMed](#)]
16. Hwang, H.Y.; Cheong, S.W. Enhanced Intergrain Tunneling Magnetoresistance in Half-Metallic CrO₂ Films. *Science* **1997**, *278*, 1607–1609. [[CrossRef](#)] [[PubMed](#)]
17. Biswas, S.; Singh, G.P.; Ram, S.; Fecht, H.J. Surface stabilized GMR nanorods of silver coated CrO₂ synthesized via a polymer complex at ambient pressure. *J. Magn. Magn. Mater.* **2013**, *339*, 175–181. [[CrossRef](#)]
18. Anwar, M.S.; Aarts, J. Anomalous transport in half-metallic ferromagnetic CrO₂. *Phys. Rev. B* **2013**, *88*, 085123. [[CrossRef](#)]
19. Corliss, L.M.; Hastings, J.M.; Nathans, R.; Shirane, G. Magnetic Structure of Cr₂O₃. *J. Appl. Phys.* **1965**, *36*, 1099–1100. [[CrossRef](#)]
20. Brown, P.J.; Forsyth, J.B.; Lelièvre-Berna, E.; Tasset, F. Determination of the magnetization distribution in Cr₂O₃ using spherical neutron polarimetry. *J. Phys. Condens. Matter* **2002**, *14*, 1957. [[CrossRef](#)]
21. Makhoulouf, S.A.; Bakr, Z.H.; Al-Attar, H.; Moustafa, M.S. Structural, morphological and electrical properties of Cr₂O₃ nanoparticles. *Mater. Sci. Eng. B* **2013**, *178*, 337–343. [[CrossRef](#)]
22. Sahoo, S.; Binek, C. Piezomagnetism in epitaxial Cr₂O₃ thin films and spintronic applications. *Philos. Mag. Lett.* **2007**, *87*, 259–268. [[CrossRef](#)]
23. McGuire, T.R.; Scott, E.J.; Grannis, F.H. Antiferromagnetism in a Cr₂O₃ Crystal. *Phys. Rev.* **1956**, *102*, 1000–1003. [[CrossRef](#)]
24. Das, P.; Bajpai, A.; Ohno, Y.; Ohno, H.; Müller, J. On the influence of nanometer-thin antiferromagnetic surface layer on ferromagnetic CrO₂. *J. Appl. Phys.* **2012**, *112*, 053921. [[CrossRef](#)]
25. Wang, Z.; Xi, L.; Yang, Y.; Li, Y.; Han, X.; Zuo, Y.; Wang, J. Spin-dependent Transport Properties of CrO₂ Micro Rod. *Nano-Micro Lett.* **2014**, *6*, 365–371. [[CrossRef](#)]
26. Bajpai, A.; Borisov, P.; Gorantla, S.; Klingeler, R.; Thomas, J.; Gemming, T.; Kleemann, W.; Büchner, B. Interface-driven magnetoelectric effects in granular CrO₂. *Eur. Phys. Lett.* **2010**, *91*, 17006. [[CrossRef](#)]
27. Bajpai, A.; Klingeler, R.; Wizen, N.; Nigam, A.K.; Cheong, S.W.; Büchner, B. Unusual field dependence of remanent magnetization in granular CrO₂: The possible relevance of piezomagnetism. *J. Phys. Condens. Matter* **2010**, *22*, 096005. [[CrossRef](#)] [[PubMed](#)]
28. Gandhi, A.C.; Wu, S.Y. Unidirectional anisotropy mediated giant memory effect in antiferromagnetic Cr₂O₃ nanorods. *RSC Adv.* **2017**, *7*, 25512–25518. [[CrossRef](#)]
29. Rietveld, H. A profile refinement method for nuclear and magnetic structures. *J. Appl. Crystallogr.* **1969**, *2*, 65–71. [[CrossRef](#)]

30. Von Dreele, R.B.; Larson, A.C. *General Structure Analysis System (GSAS)*; Los Alamos National Laboratory Report LAUR 86-748; Los Alamos National Laboratory: Los Alamos, NM, USA, 2000; p. 221.
31. Xu, X.N.; Wolfus, Y.; Shaulov, A.; Yeshurun, Y.; Felner, I.; Nowik, I.; Koltypin, Y.; Gedanken, A. Annealing study of Fe₂O₃ nanoparticles: Magnetic size effects and phase transformations. *J. Appl. Phys.* **2002**, *91*, 4611–4616. [[CrossRef](#)]
32. Gandhi, A.C.; Cheng, H.-Y.; Chang, Y.-M.; Lin, J.G. Size confined magnetic phase in NiO nanoparticles. *Mater. Res. Express* **2016**, *3*, 035017. [[CrossRef](#)]
33. Tang, Z.X.; Sorensen, C.M.; Klabunde, K.J.; Hadjipanayis, G.C. Size-dependent Curie temperature in nanoscale MnFe₂O₄ particles. *Phys. Rev. Lett.* **1991**, *67*, 3602–3605. [[CrossRef](#)] [[PubMed](#)]
34. Kaul, S.N. Static critical phenomena in ferromagnets with quenched disorder. *J. Magn. Magn. Mater.* **1985**, *53*, 5–53. [[CrossRef](#)]



© 2018 by the authors. Licensee MDPI, Basel, Switzerland. This article is an open access article distributed under the terms and conditions of the Creative Commons Attribution (CC BY) license (<http://creativecommons.org/licenses/by/4.0/>).